Thermocapillary flow near a cold wall

D. Canright
Mathematics Dept., Code MA/Ca
Naval Postgraduate School
Monterey, CA 93943
(11 June 1993)

Abstract

The thermocapillary feedback mechanism important at the edge of weld pools and other materials processes is examined through a model problem. A pool of liquid with a flat horizontal free surface is bounded on one side by a vertical solid wall, which is maintained at a cold temperature to unit depth, and at a warmer temperature below; far away the fluid is at the warmer temperature. Surface tension is a decreasing function of temperature, so that the surface thermal gradient drives flow toward the corner. When convection is vigorous, the flow compresses the thermal gradient which is driving the flow; this positive feedback results in small local length scales and high velocities near the corner. This problem is examined through a detailed scaling analysis and through numerical simulation for a range of parameters. The results show that for vigorous convection, the flow in the cold corner is locally determined.

I. INTRODUCTION

In the processing of materials, often material is melted and resolidified. Several practical processes, e.g., welding, float-zone purification, and Czochralski crystal growth, involve a pool of molten metal with a free surface, with strong temperature gradients along the surface. Convection in the molten metal is typically vigorous and significant to the results of the process, in that it affects the size and shape of the pool, the heat transfer, the mixing of solutes, and ultimately the microstructure of the finished product. The forces driving the convection include the variation of surface tension with temperature along the surface (thermocapillary forces), buoyancy forces due to thermal (and/or solutal) expansion, and electromagnetic forces in the case of arc welding or electron beam welding. However, in many cases (e.g. laser welding) thermocapillary forces predominate, and even in cases where other forces are stronger overall, there are still important regions where the thermocapillary forces may be dominant (i.e., cold corner regions: see Chen [1]).

Consequently, there have been many theoretical studies of thermocapillary flows, primarily numerical, and a few analytical (reviews are given by [2] and [3]). Cowley and Davis [4] analyzed the (two-dimensional) thermocapillary flow near a hot wall for vigorous, viscous flow (large Marangoni and Prandtl numbers); here the fluid flows up the wall then turns and flows away along the free surface, so this would be called the hot corner problem. The numerical studies of Zebib et. al. [5] of flow in a rectangular pool (2-D) with one hot and one cold wall, however, show that for moderate to small Prandtl numbers (e.g., metals) the cold corner region has by far the strongest effect on both the flow and the heat transfer. This result gives a different overall scaling than that of Cowley and Davis, although their local hot-corner scaling was validated. Other numerical studies (e.g., [6]), when a sufficiently fine mesh is used, show similar strong flow at the cold corner. Great care is necessary to insure that the small length scales of this corner region are resolved numerically; this is not always the case (as noted in [1]).

Therefore, it is imperative to develop a theoretical understanding of the dynamics of the cold corner region, where the flow along the free surface toward the cold wall compresses the thermal gradient, thereby enhancing the flow in a sort of positive feedback. Being a region of intense heat transfer, the details of the flow can affect the shape of the melt pool and the cooling rate, thus the microstructure, of the material. At the least, the dependence of the length, velocity and thermal scales on the parameters (Marangoni number, Prandtl number, Capillary number) needs to be understood in order for realistic numerical models to be designed in a way to resolve the details in this important region. But as yet, such understanding is lacking. In fact, in a recent review, Chen [1] states, "It would seem then that the structure of the cold corner flow is one of the most critical issues to be studied in the future."

To examine the feedback mechanism of the cold corner region without all the complications of the complex geometry, phase change, and time dependence inherent in real materials processing applications, a simplified model problem is considered, much like that of Cowley and Davis [4], as follows. A pool of a pure liquid has a horizontal free surface ending at a vertical wall, and the upper section of the wall is cooled; the resulting thermal gradient drives thermocapillary flow towards the cold corner. The depth and width of the pool are assumed large compared to all local length scales (which is reasonable for practical situa-

tions with high Marangoni numbers), so the pool appears semi-infinite both horizontally and vertically.

This simplified problem is still complicated, and contains most of the features of the cold corner regions in practical processes, e.g., welds. The missing features are phase change and surface deflection, both of which could modify the geometry locally (curved wall and surface), but are unlikely to change the basic structure and scaling.

The structure of the thermal and flow fields is examined below both through a detailed scaling analysis to determine the dependence on the parameters, and through numerical simulation. The numerical results validate the scaling, and for vigorous convection the cold corner flow is found to be locally determined. Hence these scalings may be useful to estimate local resolution requirements for more realistic numerical models.

II. PROBLEM STATMENT

A pool of incompressible Newtonian fluid is bounded on the left by a vertical solid wall, with the upper portion of the wall (to depth d) maintained at a cold temperature T_c, while the rest of the wall is at the hot ambient temperature T_h of the undisturbed fluid far from the corner. (See Fig. 1.) Above the horizontal free surface of the liquid is an inviscid, nonconducting gas. Surface tension is assumed strong enough to keep the free surface flat (small Capillary number), but with surface tension variations due to a linear dependence on temperature. The resulting flow is assumed to be two-dimensional and steady.

Then the equations governing the thermocapillary convection in the cold corner are conservation of mass, momentum, and energy:

$$\begin{aligned} \nabla \cdot \mathbf{u} &= 0 \\ \rho\, \mathbf{u} \cdot \nabla\, \mathbf{u} &= -\nabla\, p + \mu\, \nabla^2\, \mathbf{u} \\ \rho c_p\, \mathbf{u} \cdot \nabla\, T &= k\, \nabla^2\, T \end{aligned}$$

with the boundary conditions:

$$\begin{aligned} \text{at} \quad y = 0 \ : \quad & T_y = 0, \quad v = 0, \quad \mu u_y = \gamma T_x \\ \text{at} \quad x = 0 \ : \quad & T = \begin{cases} T_c, & y < d \\ T_h, & y > d \end{cases}, \quad u = v = 0 \\ \text{as} \quad x, y \to \infty \ : \quad & T \to T_h, \quad u,\, v \to 0 \end{aligned}$$

Here $\mathbf{u}$ is the velocity vector with components u and v in the x (horizontally rightward) and y (vertically downward) directions, p is pressure, T is temperature, ρ is density, μ is viscosity, c_p is specific heat, k is thermal conductivity, and the surface tension is assumed to be of the form $\sigma = \sigma_c - \gamma(T - T_c)$, with γ a positive constant. The boundary conditions specify that the wall is piecewise isothermal with no fluid slip, and the flat free surface is thermally insulated, with thermocapillary forcing.

The equations can be nondimensionalized by scaling lengths by d, temperature differences by $\Delta T \equiv T_h - T_c$, velocities by $u_s \equiv \gamma\, \Delta T/\mu$, and pressures by $p_s \equiv \mu u_s/d$. The resulting dimensionless equations are:

$$\nabla \cdot \mathbf{u} = 0 \tag{1}$$

$$R\,\mathbf{u} \cdot \nabla\,\mathbf{u} = -\nabla\,p + \nabla^2\,\mathbf{u} \tag{2}$$

$$M\,\mathbf{u} \cdot \nabla\,T = \nabla^2\,T \tag{3}$$

with the boundary conditions:

$$\text{at} \quad y = 0 \;: \quad T_y = 0, \quad v = 0, \quad u_y = T_x \tag{4}$$

$$\text{at} \quad x = 0 \;: \quad T = \begin{cases} -1, & y < 1 \\ 0, & y > 1 \end{cases}, \quad u = v = 0 \tag{5}$$

$$\text{as} \quad x, y \to \infty \;: \quad T \to 0, \quad u,\, v \to 0 \tag{6}$$

where $\mathbf{u}$, etc. from here on denote the dimensionless quantities. The two dimensionless parameters are the Marangoni number $M \equiv u_s d/\kappa$ and the Reynolds number $R \equiv u_s d/\nu$, where $\kappa = k/\rho c_p$ is the thermal diffusivity and $\nu = \mu/\rho$ is the kinematic viscosity. Their ratio gives the Prandtl number: $P \equiv \nu/\kappa = M/R$.

For the numerical solutions below, it is convenient to eliminate the pressure by adopting a stream-function/vorticity formulation for the flow:

$$R\,\mathbf{u} \cdot \nabla\,\omega = \nabla^2\,\omega \tag{7}$$

$$\omega = -\nabla^2\,\Psi \tag{8}$$

$$u = \Psi_y \quad , \quad v = -\Psi_x \tag{9}$$

where Ψ is the stream function and ω is the vorticity, with the flow boundary conditions

$$\text{at} \quad y = 0 \;: \quad \Psi = \Psi_x = 0, \quad \omega = -T_x \tag{10}$$

$$\text{at} \quad x = 0 \;: \quad \Psi = \Psi_x = \Psi_y = 0 \tag{11}$$

$$\text{as} \quad x, y \to \infty \;: \quad \Psi,\, \omega \to 0 \tag{12}$$

With the assumption of small Capillary number, the resulting small surface deflection can be determined as a small perturbation to the flat interface from the dimensionless normal stress condition at the surface:

$$-p + 2v_y = Ca^{-1} h_{xx} \tag{13}$$

where $Ca \equiv \gamma \Delta T/\sigma$ is the Capillary number, and the deflection h is taken positive upward (in the $-y$ direction). (Note that for the large Reynolds numbers considered in [5], the viscous stress $2v_y$ becomes negligible, and (13) reduces to their (10b).) The contact line on the wall (and on the outer boundary introduced for numerical solutions) is assumed pinned ($h = 0$), and volume is conserved globally to determine the constant reference pressure level.

III. SCALING ANALYSIS AND REGIMES OF BEHAVIOR

The structure of the thermal and flow fields can take on different forms, depending on the values of the two governing parameters, the Marangoni number M, which measures the importance of thermal convection relative to thermal diffusion, and the Prandtl number P, the ratio of viscous to thermal diffusion for the material. (Equivalently, one could use

Reynolds number $R = M/P$ as the second parameter.) Here we derive the appropriate dimensionless scales for the four different asymptotic regimes of behavior.

This scaling is based on the assumption that the thermal gradient along the free surface can be characterized by a single length scale l, which is comparable to or smaller than the imposed vertical scale of unity. In addition, let the characteristic velocity scale along the surface be U, and let δ be the vertical length scale of the velocity shear at the surface. Then the thermocapillary stress condition (4c) scales as:

$$\frac{U}{\delta} \sim \frac{1}{l} \tag{14}$$

and by continuity the vertical velocity scale in the sheared region near the surface is $V \sim U\delta/l$. In this region, the surface vorticity scales as $1/l$ by (10) and the energy and vorticity equations (3, 7) scale as:

$$M\left(\frac{U}{l} + \frac{U\delta}{l}\right) \sim \frac{1}{l^2} + 1 \tag{15}$$

$$R\left(\frac{U}{l^2} + \frac{U}{l^2}\right) \sim \frac{1}{l^3} + \frac{1}{l\delta^2} \tag{16}$$

where horizontal terms precede vertical terms, and the vertical thermal gradient is assumed to scale as unity, the imposed vertical length scale. Hence for scaling purposes, vertical convection terms can be neglected.

For small enough M, thermal convection is negligible, implying $l \sim 1$ by (15), and the thermal field is essentially conductive, decoupled from the flow. But for large enough M convection becomes important, and the strong surface flow toward the wall compresses the thermal gradient along the surface, which in turn strengthens the local driving force for the flow. This reduces the horizontal thermal length scale l to the point that thermal diffusion away from the wall balances convection toward the wall, so the local *effective* Marangoni number is order unity: $M_{eff} \equiv MUl \sim 1$. Then the externally imposed length scale (dimensional d above) is no longer directly relevant to the compressed cold corner region. (In this case, the local importance of inertia is better indicated by whether viscous or thermal diffusion is more efficient, i.e., by P rather than R.)

Similarly, for small enough R, inertia is negligible everywhere, implying $\delta \sim l$, and the flow is dominated by viscous forces. For large enough R inertial forces become dominant and viscous effects are confined to boundary layers of thickness $\delta \ll l$ along the surface and the wall, where the local effective Reynolds number $R_{eff} \equiv RU\delta^2/l \sim 1$. (Both layers are of comparable thickness because the pressure field outside the layers has the same length scale in both directions.) Hence the scaling for each regime is determined.

When the thermal field is conductive and the flow field dominated by viscous forces ($M \ll 1$ and $R \ll 1$, or $P \gg M$), all three scales are of order unity: $l \sim 1$, $\delta \sim 1$, $U \sim 1$. Thus in this case (only), the scaling used in the nondimensionalization is appropriate everywhere. Within this regime, the solution is fully two-dimensional with no fine structure and is nearly independent of the parameters (rather, it is determined by the boundary conditions).

For the conductive case with inertial flow, the additional resistance of inertia reduces both the velocity scale and the viscous length scale: $U \sim \delta \sim R^{-\frac{1}{3}}$ (while $l \sim 1$ still). This

reduced velocity also reduces the effective Marangoni number, such that this regime applies when $M \ll R^{\frac{1}{3}}$, or $M \ll P^{-\frac{1}{2}}$, with $R \gg 1$, or $P \ll M$. (Note that this gives the same boundary layer scaling as Zebib et al. [5] except for an error on the passive wall layers, as pointed out by Chen [1].) Here the vorticity generated by the shear stresses on the surface and the wall are confined to the thin boundary layers.

When thermal convection is important but inertia is not ($M \gg 1$ and $P \gg 1$), surface thermal variations are compressed to a narrow region, beyond which the thermocapillary forcing is small, so $\delta \sim l \sim M^{-1}$ and $U \sim 1$. However, as the numerical results show, the strong inward flow along the surface turns downward and *away* from the no-slip wall (and weakens rapidly with distance), such that *no* thermal boundary layer is formed on the wall; rather, vertical and horizontal variations are comparable.

The most important regime for materials processing is where thermal convection is important and $P \ll 1$, the latter being generally true for metals. In this case, within the compressed thermal region there are thin viscous boundary layers along the surface and wall. Then $l \sim M^{-1}P^{-\frac{1}{2}}$, $\delta \sim M^{-1}$, and $U \sim P^{\frac{1}{2}}$, i.e., the additional resistance of inertia decreases the velocity scale and thus increases the thermal length scale by a factor of $P^{\frac{1}{2}}$ relative to the purely viscous case. Again the reduced velocity changes the thermal convection scaling, and large Marangoni number here means $M \gg P^{-\frac{1}{2}}$.

The approximate divisions between the four asymptotic regimes and their scalings are summarized in Table I. For a material of small P, as M is increased from zero, at first the temperature field is conductive and the flow dominated by viscous forces, then the flow becomes primarily inertial and viscous boundary layers form, and finally thermal convection becomes important, shrinking all local length scales in the corner.

A. Viscous Corner Region

There is a region in the corner, for any M and P, where viscous stresses from the wall limit the flow and both inertia and thermal convection are negligible, so the temperature along the surface is approximately linear. Locally the thermocapillary stress is constant, and the flow is given by a similarity solution ([7], although the published version contains errors).

If the flat free surface makes an angle α with the solid wall, then a constant unit surface shear stress toward the corner gives

$$\Psi(r,\theta) = \frac{r^2}{4}\,\frac{[(\sin 2\alpha - 2\alpha)(\cos 2\theta - 1) - (\cos 2\alpha - 1)(\sin 2\theta - 2\theta)]}{\sin 2\alpha - 2\alpha\cos 2\alpha}$$

where r and θ are polar coordinates, with θ increasing from the wall to the free surface (see Fig. 1). In the particular case here, $\alpha = \frac{\pi}{2}$, and

$$\Psi(r,\theta) = r^2\left[\frac{1}{4}(1-\cos 2\theta) + \frac{1}{2\pi}(\sin 2\theta - 2\theta)\right]$$

$$\mathbf{u} = r\left\{\left[\frac{1}{2}\sin 2\theta + \frac{1}{\pi}(\cos 2\theta - 1)\right]\hat{r} - \left[\frac{1}{2}(1-\cos 2\theta) + \frac{1}{\pi}(\sin 2\theta - 2\theta)\right]\hat{\theta}\right\}$$

$$\omega = 1 - \frac{4}{\pi}\theta$$
$$p - p_0 = \frac{4}{\pi}\ln r$$

where $\hat{r}$ and $\hat{\theta}$ are unit vectors in the coordinate directions, and p_0 is some reference pressure.

This is the form of the flow in the cold corner on the smallest length scale, where all the above flow quantities would be multiplied by the surface stress $T_x(0,0)$ (which scales as $1/l$). The velocity grows linearly with distance r from the corner and the local length scale is r, which can be used to estimate the range over which the similarity solution is applicable. For the two viscous-flow regimes mentioned above, the linear-temperature approximation requires $r \ll l$, so for the conductive regime $r \ll 1$ while for the convective regime $r \ll M^{-1}$. For the two inertial-flow regimes, the more restrictive condition is that locally inertia is negligible, and the local velocity scale is r/l, so we must have $r^2 \ll l/R$; in the conductive regime this implies $r \ll R^{-\frac{1}{2}}$, while in the convective regime the range is $r \ll P^{\frac{1}{4}}M^{-1}$, or $r/l \ll P^{\frac{3}{4}}$. These scales are also summarized in Table I.

This gives an estimate of the resolution required for a numerical model to resolve all the details of the cold corner flow. Because of the corner singularity in p and ω, spectral methods would be inappropriate; instead, finite-difference or finite-element methods could be used. Then provided that the first grid point is in the similarity range, no details of the velocity field in the corner should be lost. In addition, the similarity form may be useful as a "matching" type boundary condition for the singularity at the origin.

IV. NUMERICAL METHODS

While the idealized problem considers the cold corner in isolation from other boundaries and effects, for computational purposes a finite domain was required. A square domain was used, each side five times the imposed thermal length scale. It was hoped this would be large enough so that the "outer" boundaries would have only small effects on the cold corner feedback mechanism, as the thermal gradient along the surface decays quickly with distance. These boundaries were made isothermal, impenetrable, and shear-free, and hence constrain both the thermal and flow fields, enforcing recirculation and preventing long thermal plumes. (Diagonal plumes were seen to form in calculations for the $R = 0$ case using a Green's function method and different outer boundary conditions; see [8].)

To calculate the steady state for various values of M and P, the time-dependent finite-difference equations were explicitly stepped in time until steady state was reached. At each time step, the convection-diffusion equations for temperature (3) and vorticity (7) were solved by the Alternating-Direction Implicit (ADI) scheme [9], where the convective terms were evaluated by the Eulerian-Lagrangian Method (ELM, see [10]) using the velocity field from the (old) stream function and upwind bilinear interpolation. (The ADI method avoids diffusive numerical instability, so the time step is only limited by convective stability.) After several time steps, the stream function was updated by solving the Poisson equation (8) using Gauss-Seidel iteration with Successive Over-Relaxation (SOR). Steady state was assumed when the pointwise RMS change in stream function fell below a certain tolerance.

A non-uniform Cartesian grid was employed. Then using a three-point difference scheme, only first-order accuracy is possible for the second derivatives; the differencing employed

becomes second-order accurate in the limit of uniform spacing. Specifically, the following one-dimensional difference formulae were used (derived from Taylor series):

$$f' = \frac{-dx_+}{dx_-(dx_+ + dx_-)}\, f_- + \frac{dx_+ - dx_-}{dx_+ dx_-}\, f + \frac{dx_-}{dx_+(dx_+ + dx_-)}\, f_+ + O(f''' dx_+ dx_-)$$

$$f'' = \frac{2}{dx_-(dx_+ + dx_-)}\, f_- + \frac{-2}{dx_+ dx_-}\, f + \frac{2}{dx_+(dx_+ + dx_-)}\, f_+ + O(f'''(dx_+ - dx_-))$$

where dx_- and dx_+ are the distances to the grid points below and above the current point, with f_- and f_+ the corresponding values of the function.

The grid spacing in each direction was chosen to have a closely packed region of uniform spacing by the surface or wall, a widely spaced region of uniform spacing near the outer boundaries, and in between a region of smoothly (exponentially) changing spacing. This was generated by applying the following function to a uniform grid (in ξ, say):

$$\frac{x}{x_{max}} = f(\xi) = \frac{1}{D} \times \begin{cases} \ln r\, \xi, & 0 \le \xi < \xi_1 \\ \ln r\, \xi_1 + (\xi_2 - \xi_1)\,(r^{(\xi-\xi_1)/(\xi_2-\xi_1)} - 1), & \xi_1 \le \xi < \xi_2 \\ D - r \ln r\, (1 - \xi), & \xi_2 \le \xi \le 1 \end{cases}$$

where r is the ratio of outer spacing to inner spacing, ξ_1 and ξ_2 are parameters delineating the three regions, $D = (r-1)(\xi_2 - \xi_1) + \ln r(r + \xi_1 - r\xi_2)$ is the common denominator, and x_{max} is the position of the outer boundary. Table II shows the grid spacing used in each case.

It was found that, even when the time step easily satisfied convective stability requirements, nonetheless numerical instabilities sometimes developed in the vorticity near the wall. Several different formulations for the wall boundary condition on vorticity were tried, to no avail. However, by under-relaxing the changes in wall vorticity, only during the initial adjustment period, the instability was eliminated. The formula used to calculate the vorticity at the wall (without under-relaxation) from the stream function is

$$\omega_0 = \frac{2(\Psi_1 - \Psi_2)}{x_2^2 - x_1^2} \quad + O(\Psi''' x_2)$$

where subscripts 0, 1, and 2 refer to the wall and the first two grid points. While only first-order, this formulation is independent of Ψ_0 and thus avoids re-using the boundary condition for Ψ.

V. RESULTS AND DISCUSSION

Numerical solutions were calculated for three different Prandtl numbers (P = 0.01, 1, 100) over a wide range of Marangoni numbers, as indicated in Table II, to explore the various regimes of behavior. A solution representative of the conductive viscous regime is shown in Fig. 2. (Note: in all plots, no curve smoothing was used, only straight-line interpolation.) The vorticity decays with distance from the discontinuity in the corner, and the velocity

is strongest along the free surface. The thermal field is close to the conduction solution for a quarter plane, but is slightly compressed by the outer isothermal boundaries. (The temperature discontinuity on the wall at $y = 1$, introduced by the boundary conditions, plays no dynamical role, other than to set an overall thermal length scale.)

A convective viscous solution is shown in Fig. 3. Vigorous convection along the surface compresses the surface thermal gradient to a small region, but no thermal boundary layer forms along the wall. Rather, because the flow out of the corner is not only downward but also outward, the fluid cooled by the upper portion of the wall is swept *diagonally* downward, away from the warm lower portion of the wall, giving a sort of diagonal thermal plume. (This diagonal plume effect is much clearer with less restrictive outer boundary conditions, as are possible with a Green's function approach for $R = 0$; see [8]. This effect seems due largely to the direction of the strong convection out of the corner; for smaller P the flow has very little outward component.) The vorticity is confined to a small region in the corner, where its distribution is qualitatively similar to the conductive viscous case. The maximum surface velocity occurs very near the wall, and decays quickly with distance (see Fig. 6b).

A conductive solution where inertia is important is shown in Fig. 4, with $P = 0.01$. The vorticity is confined to relatively thin layers along the surface and the wall, and while the thermal is virtually the same as in Fig. 2, the surface velocity maximum occurs relatively close to the corner (see Fig. 7b). (On the large scale, the flow separates from the wall, giving a weak counter-circulation at the bottom, not shown.)

Fig. 5 shows a convective inertial solution, again with $P = 0.01$. The vorticity generated on the surface and wall is convected along very thin boundary layers where the flow is rapid, qualitatively like a narrow jet impinging on a rigid wall. The surface layer extends only as far as the compressed thermal gradient. Outside these layers the flow is slower, but still strong enough to modify the thermal field. Whether a thermal boundary layer would form at higher M is not clear from these results, but seems likely. (Here $R = 10^6$; obtaining convergent solutions became increasingly difficult as M was raised. Also, the counter-circulation has grown to fill the bottom half of the domain, not shown.)

The effects of increasing M on surface velocities, temperatures and interface deflections (calculated from the small-Ca linearized equation 13) are shown in Fig. 6 for $P = 100$ and Fig. 7 for $P = 0.01$. (Surface profiles for $P = 1$ are similar to those for $P = 100$.) The main features are summarized in Fig. 8. While the thermal gradient, which forces the flow, becomes stronger, it also acts over a decreasing range, localized near the wall. The result on the flow is that the surface velocity maximum moves close to the wall, but the maximum speed remains roughly constant for large P. For small P, increasing inertial resistance lowers the maximum speed until the thermal gradient grows stronger. The surface deflection is upward near the wall, then downward (and may go upward again as necessary to conserve volume), with the local maximum moving closer to the wall with increasing M, and, for small P, becoming overwhelmed by the growing downward deflection.

The results agree well with the scaling analysis, based on the following comparisons: the wall thermal gradient $|T_x(0,0)|$ indicates the inverse of the thermal length scale l, the maximum speed $|u|_{max}$ gives the velocity scale U, and the position x_{max} of the velocity maximum indicates the viscous length scale δ. Lines of slope 1 and -1 show the expected behavior of T_x and x_{max} in the convective regimes, and a line of slope $-\frac{1}{3}$ in Fig. 8c shows the expected behavior of u_{max} and x_{max} in the conductive inertial regime for small P;

elsewhere the quantities are expected to remain roughly constant. The data clearly show the transitions between the regimes. The scaling estimates of the Marangoni numbers of transition (see Table I) seem to be consistently low by a numerical factor of roughly 20; for example, the scaling predicts the transition to convective behavior for large P at about $M = 1$, while figures 8a,b show the transition at about $M = 20$.

The assumption that the behavior in the cold corner is locally determined for the convective regimes can be examined by rescaling the results based on the scaling analysis, as shown in Figure 9. For $P = 100$, the convective viscous solutions locally appear the same, when rescaled, at least as far as surface velocities and temperatures, and similarly for the convective inertial solutions with $P = 0.01$. (In both cases, the solution that sticks out is for the lowest M included, for which the transition to fully convective behavior is apparently not complete. For $P = 0.01$, solutions for $M = 30,000$ and $M = 50,000$ had small separated regions on the wall near the surface that disturbed the local behavior; hence these were excluded.)

VI. CONCLUSIONS

The practical importance of thermocapillary convection in materials processing, along with the complications inherent in typical processes (e.g. curved interfaces, phase change, etc.), ensure that numerical simulations will remain one of the main theoretical tools for understanding such systems. This work predicts, *a priori*, the resolution requirements for such numerical models to accurately represent the high heat transfer and rapid velocity variations in the cold corner region.

The structure of the corner depends on two dimensionless parameters indicating the driving force for convection and relative importance of viscosity: the Marangoni number M (based on the overall temperature difference, overall thermal length scale, and material properties) and the Prandtl number P (a material property). Hence there are four asymptotic regimes depending on whether thermal convection and inertial forces are locally important. For large-P materials (e.g., organics), the flow is dominated by viscous forces, and for large M the surface thermal variations are compressed, i.e., the local length scale is decreased (and heat transfer increased). For small-P materials (e.g., metallics), inertia becomes important before thermal convection with increasing M, and thin viscous boundary layers form along the surface and the wall, within the thermal region. When M is large (compared to $P^{-1/2}$), three levels of length scales must be resolved (overall, thermal, and viscous), a severe requirement on numerical models. Resolution of flow details is assured by a grid fine enough to reach the self-similar behavior at the corner singularity.

The scaling was derived from a simple problem designed to isolate the feedback mechanism of the cold corner. Numerical calculations (where the corner is necessarily less isolated due to the finite domain) illustrate the changing structure of the cold corner and show the details of the transitions between the asymptotic regimes. The numerical results are consistent with the scaling analysis. In particular, for fully convective flow the corner behavior is *locally* determined; increasing the global Marangoni number merely decreases the local length scale to give a local effective Marangoni number of unity. Hence the boundary conditions on the outer boundaries become irrelevant to the local feedback mechanism in the

cold corner, and the behavior shown in Fig. 3 and Fig. 5 may be considered characteristic, for low and high P respectively.

One surprising result, in contrast with the hot corner problem of Cowley and Davis [4], is that no thermal boundary layer forms for large P. This difference is due to the surface forcing being limited to a relatively concentrated region in the cold corner, while for the hot corner the forcing is distributed over an broad region, the horizontal thermal variations being extended by convection. (For small P, the numerical results are inconclusive about whether a laminar thermal boundary layer forms for sufficiently large M.)

To compare with the numerical results of Zebib et al. [5] for $P = 1$, note the different boundary conditions: their domain had a pool between a hot and a cold no-slip wall, with an insulated no-slip bottom. Then even when the cold corner was highly compressed, there were still significant thermal variations along most of the surface due to the hot wall, so the overall scaling is similar to the conductive inertial case here. And apparently even their cold corner was modified by the external bulk flow, for their maximum vorticity scaled as $\omega \propto M^{2/3}$, whereas here $\omega \propto M$. Hence one important question remaining is under what global conditions can the cold corner be considered locally determined.

In real materials processes, the surface is free to deflect, and the position and shape of the solid-liquid interface depends on the thermal field. These effects greatly complicate the problem geometrically, yet the dominant dynamic balance should remain that considered here.

ACKNOWLEDGMENTS

This work was supported by the Office of Naval Research, Materials Division (contract N0001492WR24009). The author is grateful to Stephen H. Davis for suggesting this topic.

REFERENCES

[1] M. M. Chen, in *Interdisciplinary Issues in Materials Processing and Manufacturing*, ASME, edited by S. K. Samanta *et al.* (ASME, New York, 1987), pp. 541–557.

[2] S. Ostrach, Ann. Rev. Fluid Mech. **14**, 313 (1982).

[3] S. H. Davis, Ann. Rev. Fluid Mech. **19**, 403 (1987).

[4] S. J. Cowley and S. H. Davis, J. Fluid Mech. **135**, 175 (1983).

[5] A. Zebib, G. M. Homsy, and E. Meiburg, Phys. Fluids **28**, 3467 (1985).

[6] R. Zehr, M. M. Chen, and J. Mazumder, in *ASME National Heat Transfer Conference, Pittsburgh, PA* (ASME, New York, 1987), paper No. 87-HT-229.

[7] H. K. Moffatt, J. Fluid Mech. **16**, 1 (1964).

[8] M. R. Huber and D. Canright, A Green's Function Approach to Thermocapillary Flow in a Cold Corner, submitted to Numerical Heat Transfer.

[9] D. A. Anderson, J. C. Tannehill, and R. H. Pletcher, *Computational Fluid Mechanics and Heat Transfer* (Hemisphere Publishing Corporation, New York, 1984).

[10] R. T. Cheng, V. Casulli, and S. N. Milford, Water Resources Research **20**, 944 (1984).

FIGURES

FIG. 1. Problem Formulation: a liquid quarter-space is bounded above by a flat free surface subject to thermocapillary forcing, and is bounded on the left by a rigid vertical wall, at temperature T_c to depth d and at the warmer temperature T_h below, which is also the ambient temperature of the undisturbed fluid far away.

FIG. 2. Results for $P = 100$, $M = 0.1$: isotherms (dark gray), streamlines (thin, black) and vorticity contours (light gray) for a numerical solution dominated by thermal diffusion and viscous forces. The temperature discontinuity on the wall (on the left) is due to the chosen boundary conditions and plays no dynamical role other than to set the thermal length scale. In contrast, the vorticity discontinuity where the free surface (top) meets the wall is inherent to the thermocapillary problem. The bottom and right boundaries ($y = 5$, $x = 5$) constrain the recirculating streamlines.

FIG. 3. Results for $P = 100$, $M = 1000$, detail ($0 < x < 2$, $0 < y < 2$): a convective, viscous solution. Strong surface flow compresses the surface thermal gradient into the cold corner, but no boudary layer forms on the wall. The length scale of vorticity variations is that of the surface thermal gradient. The maximum velocity occurs on the surface near the wall.

FIG. 4. Results for $P = 0.01$, $M = 30$, detail ($0 < x < 2$, $0 < y < 2$): conductive, with inertial flow. Vorticity is convected in fairly thin layers on the surface and the wall.

FIG. 5. Results for $P = 0.01$, $M = 10,000$, detail ($0 < x < 0.5$, $0 < y < 0.5$): a convective, inertial solution. Within the compressed thermal field, vorticity is confined to thin viscous boundary layers.

FIG. 6. Surface Profiles, $P = 100$, $M = 1$, 10, 100, 1000: (a) Surface temperature ($-T$) as function of x. For large M, outside the corner the temperature is an order of magnitude smaller than the wall temperature and nearly linear. (b) Surface speed ($-u$). The corner length scale decreases (but the velocity scale does not) with increasing M. (c) Free-surface deflection: scaled surface height (h/Ca) from the small-Ca linearized equation 13.

FIG. 7. Surface Profiles, $P = 0.01$, $M = 0.01$, 0.1, 1, 10, 100, 1000, 10,000: (a) Surface temperature. Again, for large M the temperature outside the corner is an order of magnitude smaller than the wall temperature. (b) Surface speed. Both the corner length scale and the velocity scale decrease with increasing M. (c) Free-surface deflection (from 13).

FIG. 8. Summary of Numerical Scales: wall temperature gradient $|T_x|$ (diamonds), maximum speed $|u|_{max}$ (triangles), and position x_{max} of maximum speed (stars), as functions of Marangoni number M, from numerical solutions. Lines of slope 1, -1, and -1/3 are shown for comparison with scaling analysis. (a) $P = 100$. (b) $P = 1$. (c) $P = 0.01$.

FIG. 9. Rescaled Surface Profiles: temperature and velocity profiles for convective regimes, with x axis rescaled by M. The collapse of the data indicates the behavior in the cold corner is locally determined. (a) viscous case: $P = 100$; $M = 200$, 300, 500, 700, 1000. (b) inertial case: $P = 0.01$; $M = 3000$, 5000, 7000, 10,000, 20,000.

TABLES

TABLE I. Summary of theoretical scales in the cold corner: thermal length l, viscous thickness δ, surface speed U, and bound r on extent of viscous corner similarity solution.

Regime		Scales			
Type	Limits	l	δ	U	r
cond. visc.	$M \ll 1,\ P \gg M$	1	1	1	1
conv. visc.	$M \gg 1,\ P \gg 1$	M^{-1}	M^{-1}	1	M^{-1}
cond. inert.	$P \ll M \ll P^{-\frac{1}{2}},\ P \ll 1$	1	$M^{-\frac{1}{3}}P^{\frac{1}{3}}$	$M^{-\frac{1}{3}}P^{\frac{1}{3}}$	$M^{-\frac{1}{2}}P^{\frac{1}{2}}$
conv. inert.	$M \gg P^{-\frac{1}{2}},\ P \ll 1$	$M^{-1}P^{-\frac{1}{2}}$	M^{-1}	$P^{\frac{1}{2}}$	$M^{-1}P^{\frac{1}{4}}$

TABLE II. Grid spacing used in computations. For each P and M the total number of grid points (in each direction, including boundaries) is $npts$, the minimum spacing is h_{min} (where the whole domain is 5 units wide), and the ratio r of maximum to minimum spacing is h_{max}/h_{min}. For large M, the minimum spacing should be inversely proportional to M to preserve resolution of corner details, i.e., $M\,h_{min}$ should be roughly constant.

P	M	$npts$	h_{min}	h_{max}/h_{min}	$M\,h_{min}$
0.01	0.01	41	0.024251	10	0.00024
0.01	0.03	41	0.024251	10	0.00073
0.01	0.1	41	0.024251	10	0.0024
0.01	0.3	41	0.024251	10	0.0073
0.01	1	41	0.024251	10	0.024
0.01	3	41	0.024251	10	0.073
0.01	10	41	0.024251	10	0.24
0.01	30	41	0.024251	10	0.73
0.01	100	61	0.010037	20	1.0
0.01	300	61	0.010037	20	3.0
0.01	1000	61	0.004280	40	4.3
0.01	2000	61	0.002301	70	4.6
0.01	3000	61	0.002301	70	6.9
0.01	5000	61	0.001112	150	5.6
0.01	7000	61	0.001112	150	7.8
0.01	10,000	61	0.001112	150	11.1
0.01	20,000	101	0.000301	300	6.0
0.01	30,000	121	0.000358	300	10.8
0.01	50,000	121	0.000155	600	7.8
1	0.01	31	0.092069	3	0.00092
1	1	31	0.092069	3	0.092
1	3	31	0.092069	3	0.28
1	10	31	0.092069	3	0.92
1	30	31	0.092069	3	2.8
1	100	51	0.027068	7	2.8
1	200	51	0.027068	7	5.4
1	300	51	0.016573	15	5.0
1	500	51	0.007977	25	4.0
1	1000	61	0.004280	40	4.3
100	0.1	31	0.092069	3	0.0092
100	0.3	31	0.092069	3	0.028
100	1	31	0.092069	3	0.092
100	3	31	0.092069	3	0.28
100	5	31	0.092069	3	0.46
100	10	31	0.092069	3	0.92
100	30	41	0.044737	5	1.3
100	50	41	0.044737	5	2.2
100	100	41	0.044737	5	4.5
100	200	51	0.020561	10	4.1

100	300	61	0.010037	20	3.0
100	500	81	0.004949	40	2.5
100	700	81	0.004949	40	3.5
100	1000	81	0.004949	40	4.9

Figures for "Thermocapillary Flow Near a Cold Wall"

David Canright

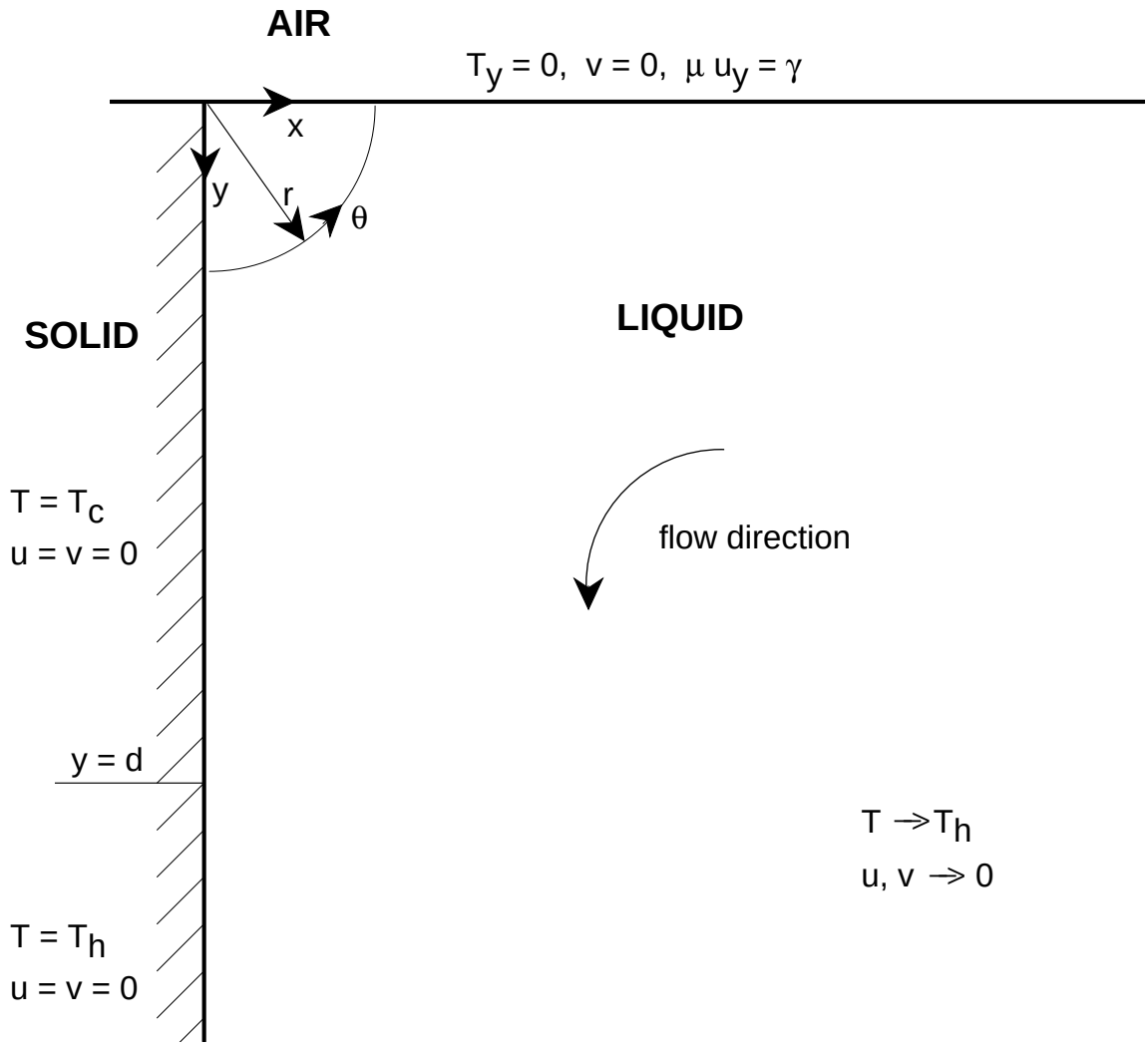

Figure 1: Problem Formulation: a liquid quarter-space is bounded above by a flat free surface subject to thermocapillary forcing, and is bounded on the left by a rigid vertical wall, at temperature T_c to depth d and at the warmer temperature T_h below, which is also the ambient temperature of the undisturbed fluid far away.

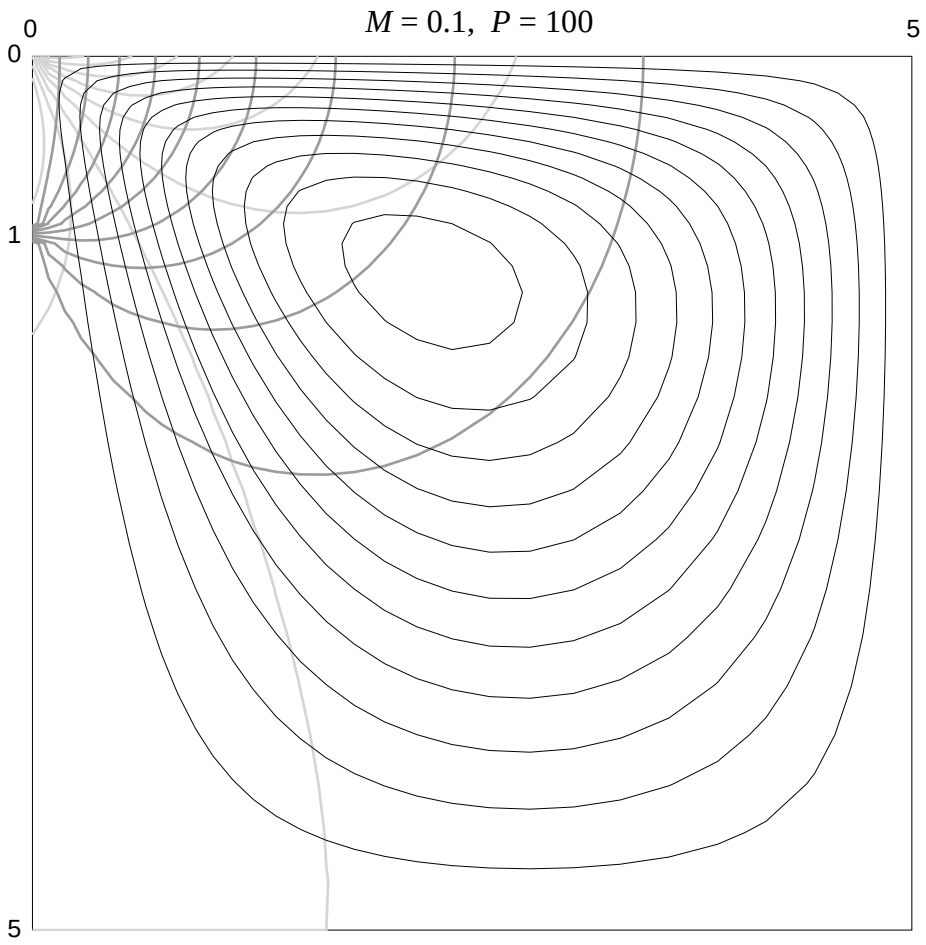

Figure 2: Results for $P = 100$, $M = 0.1$: isotherms (dark gray), streamlines (thin, black) and vorticity contours (light gray) for a numerical solution dominated by thermal diffusion and viscous forces. The temperature discontinuity on the wall (on the left) is due to the chosen boundary conditions and plays no dynamical role other than to set the thermal length scale. In contrast, the vorticity discontinuity where the free surface (top) meets the wall is inherent to the thermocapillary problem. The bottom and right boundaries ($y = 5$, $x = 5$) constrain the recirculating streamlines.

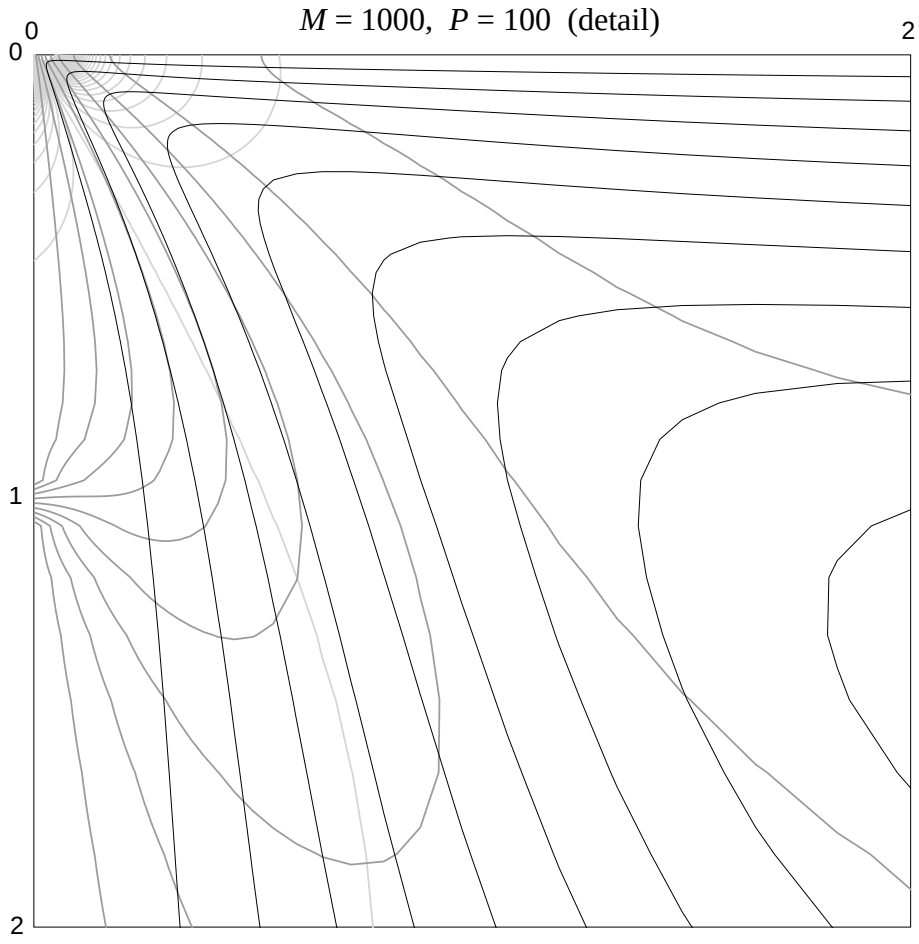

Figure 3: Results for $P = 100$, $M = 1000$, detail ($0 < x < 2$, $0 < y < 2$): a convective, viscous solution. Strong surface flow compresses the surface thermal gradient into the cold corner, but no boudary layer forms on the wall. The length scale of vorticity variations is that of the surface thermal gradient. The maximum velocity occurs on the surface near the wall.

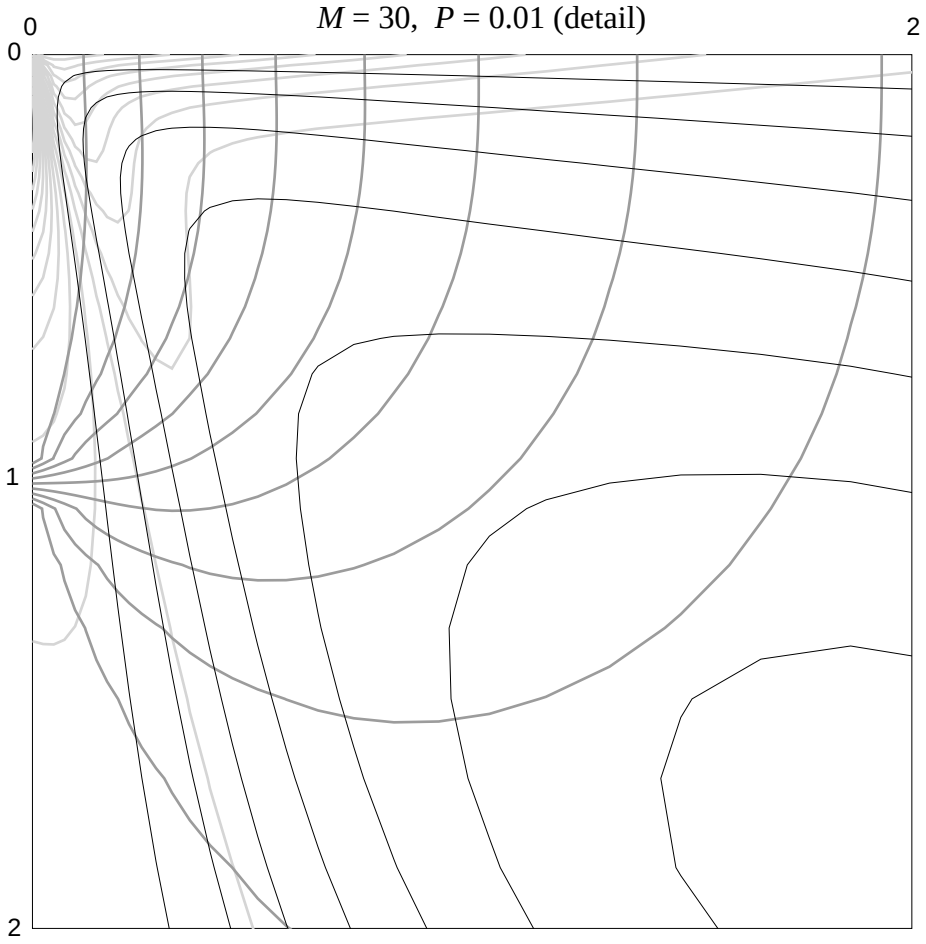

Figure 4: Results for $P = 0.01$, $M = 30$, detail ($0 < x < 2$, $0 < y < 2$): conductive, with inertial flow. Vorticity is convected in fairly thin layers on the surface and the wall.

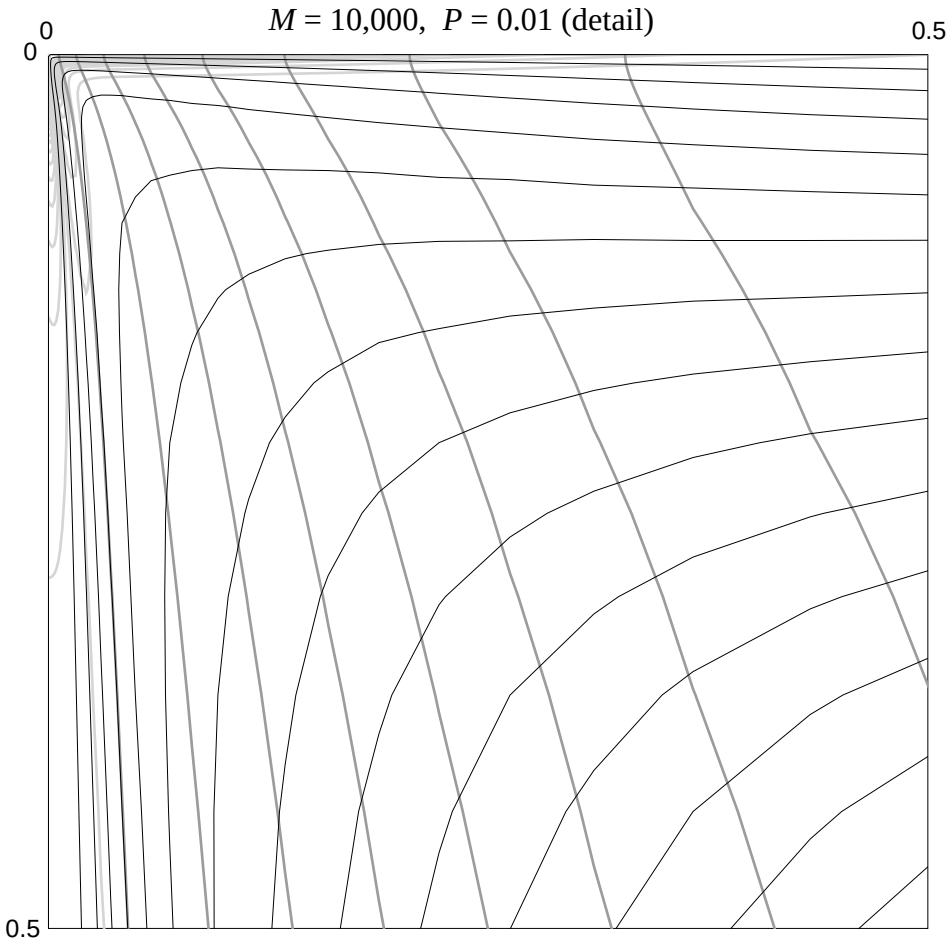

Figure 5: Results for $P = 0.01$, $M = 10,000$, detail ($0 < x < 0.5$, $0 < y < 0.5$): a convective, inertial solution. Within the compressed thermal field, vorticity is confined to thin viscous boundary layers.

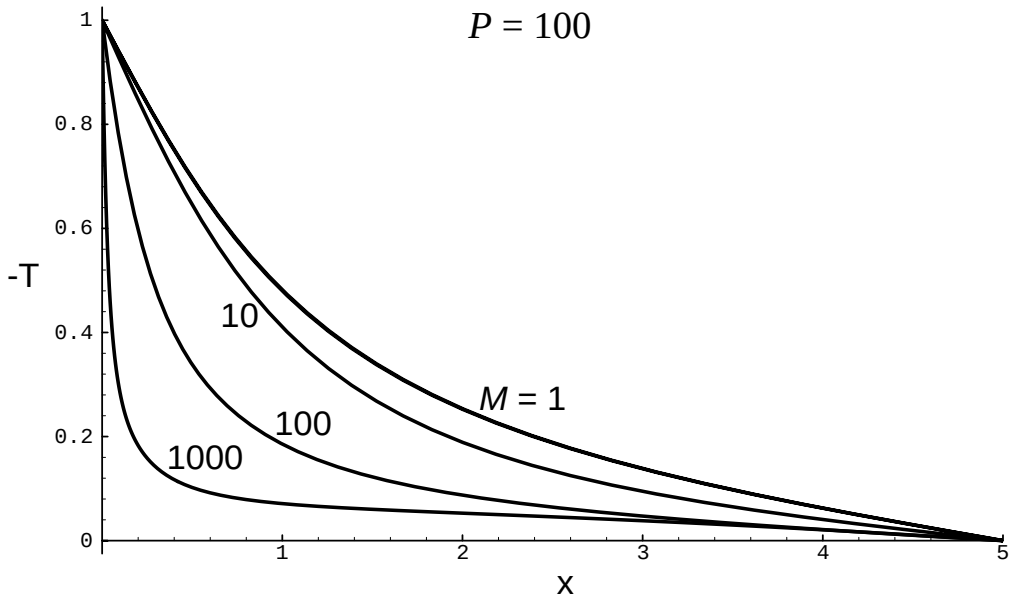

Figure 6: Surface Profiles, $P = 100$, $M = 1$, 10, 100, 1000: (a) Surface temperature $(-T)$ as function of x. For large M, outside the corner the temperature is an order of magnitude smaller than the wall temperature and nearly linear.

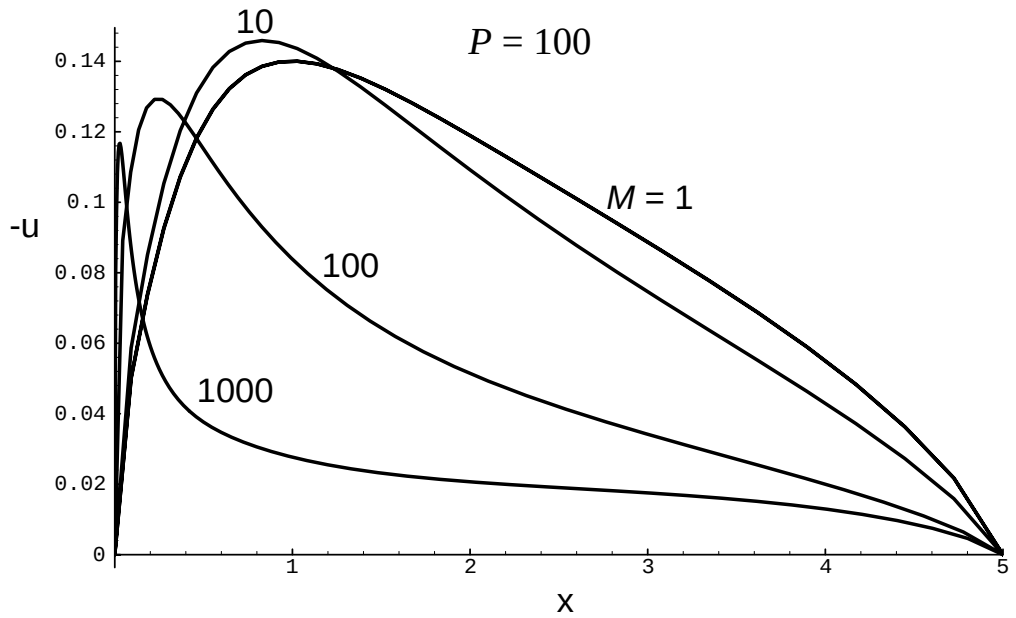

Figure 6: (b) Surface speed $(-u)$. The corner length scale decreases (but the velocity scale does not) with increasing M.

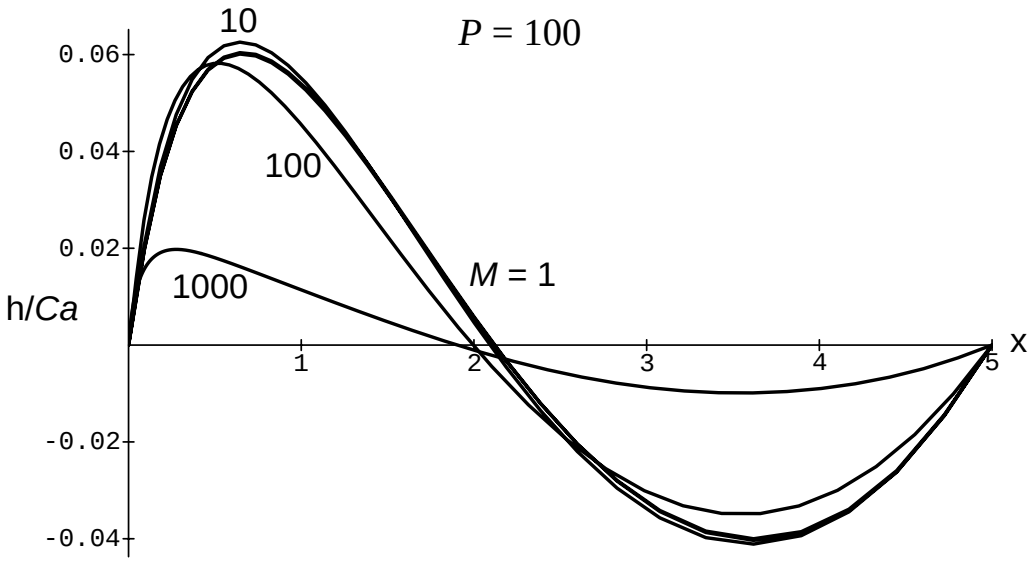

Figure 6: (c) Free-surface deflection: scaled surface height (h/Ca) from the small-Ca linearized equation (13).

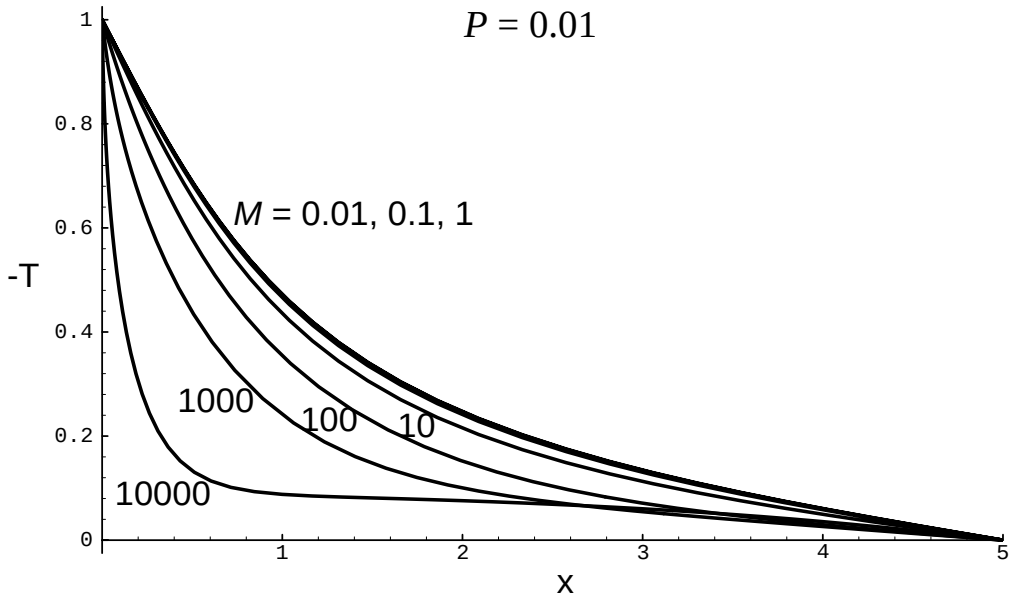

Figure 7: Surface Profiles, $P = 0.01$, $M = 0.01$, 0.1, 1, 10, 100, 1000, 10,000: (a) Surface temperature. Again, for large M the temperature outside the corner is an order of magnitude smaller than the wall temperature.

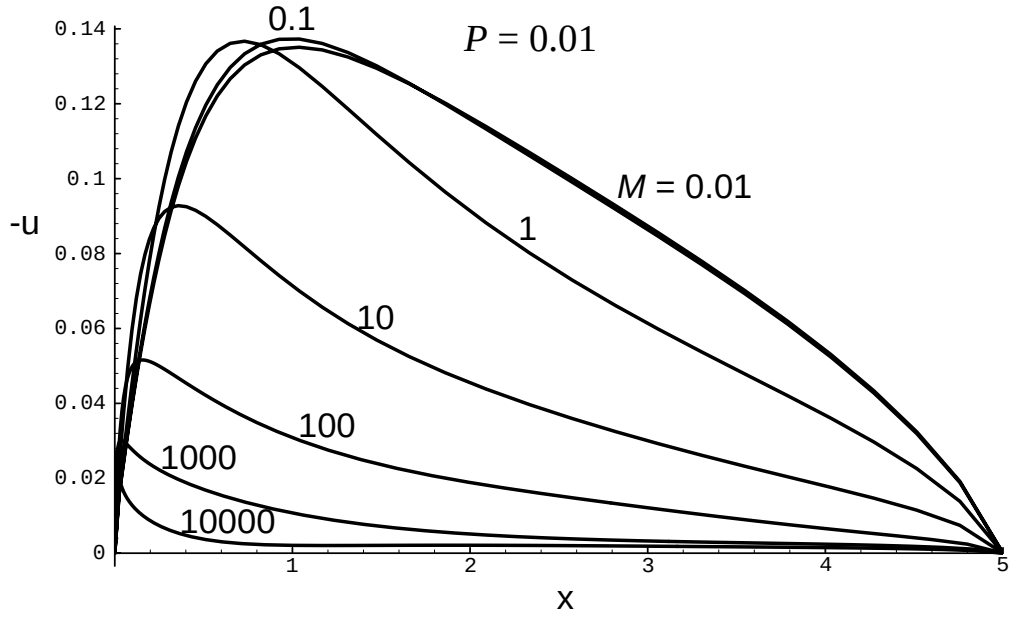

Figure 7: (b) Surface speed. Both the corner length scale and the velocity scale decrease with increasing M.

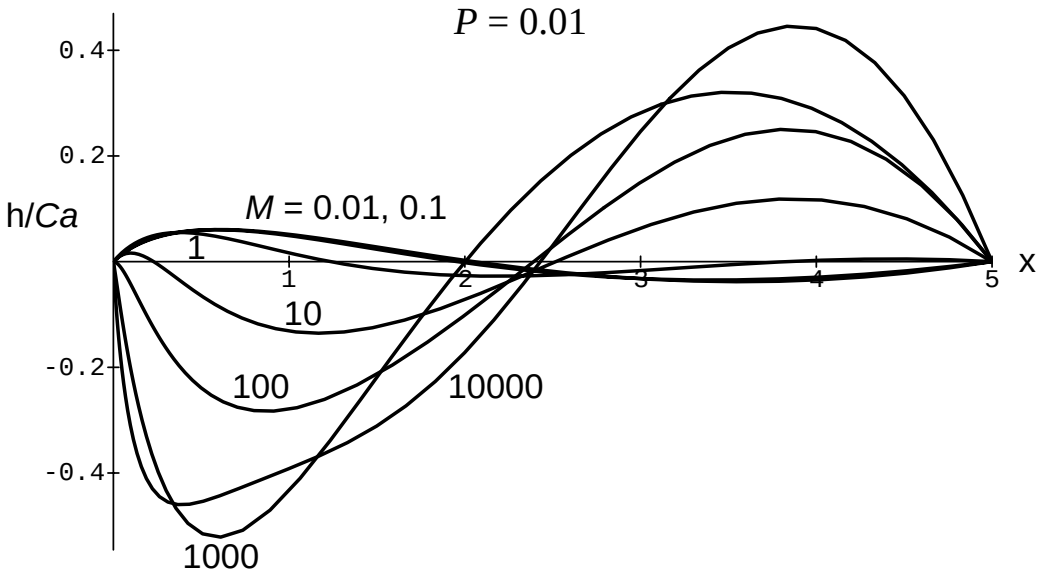

Figure 7: (c) Free-surface deflection [from (13)].

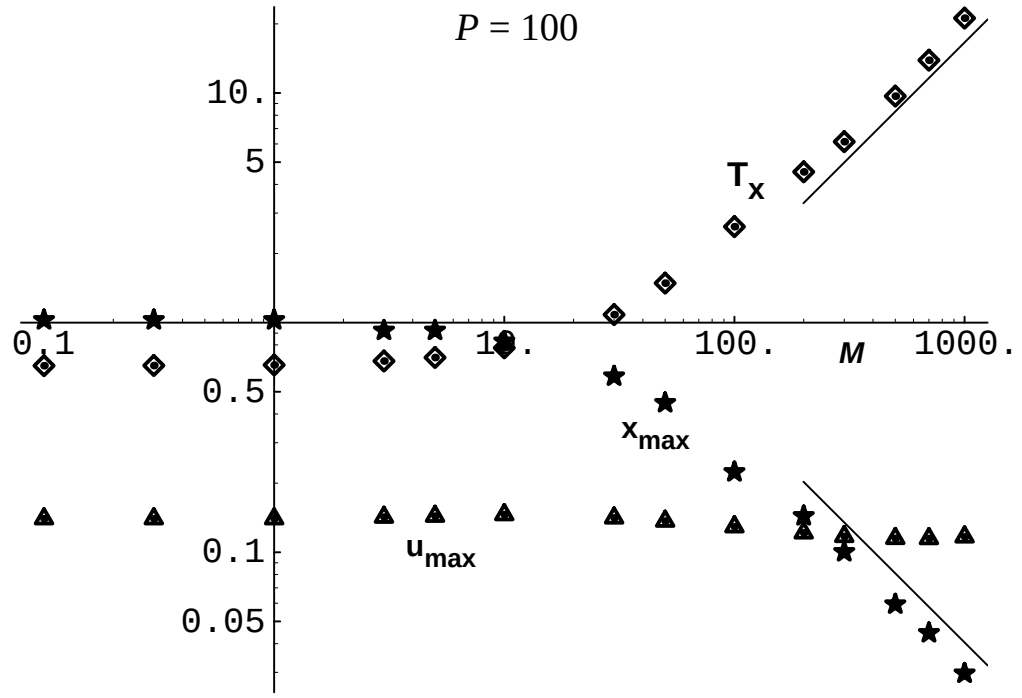

Figure 8: Summary of Numerical Scales: wall temperature gradient $|T_x|$ (diamonds), maximum speed $|u|_{max}$ (triangles), and position x_{max} of maximum speed (stars), as functions of Marangoni number M, from numerical solutions. Lines of slope 1, -1, and -1/3 are shown for comparison with scaling analysis. (a) $P = 100$.

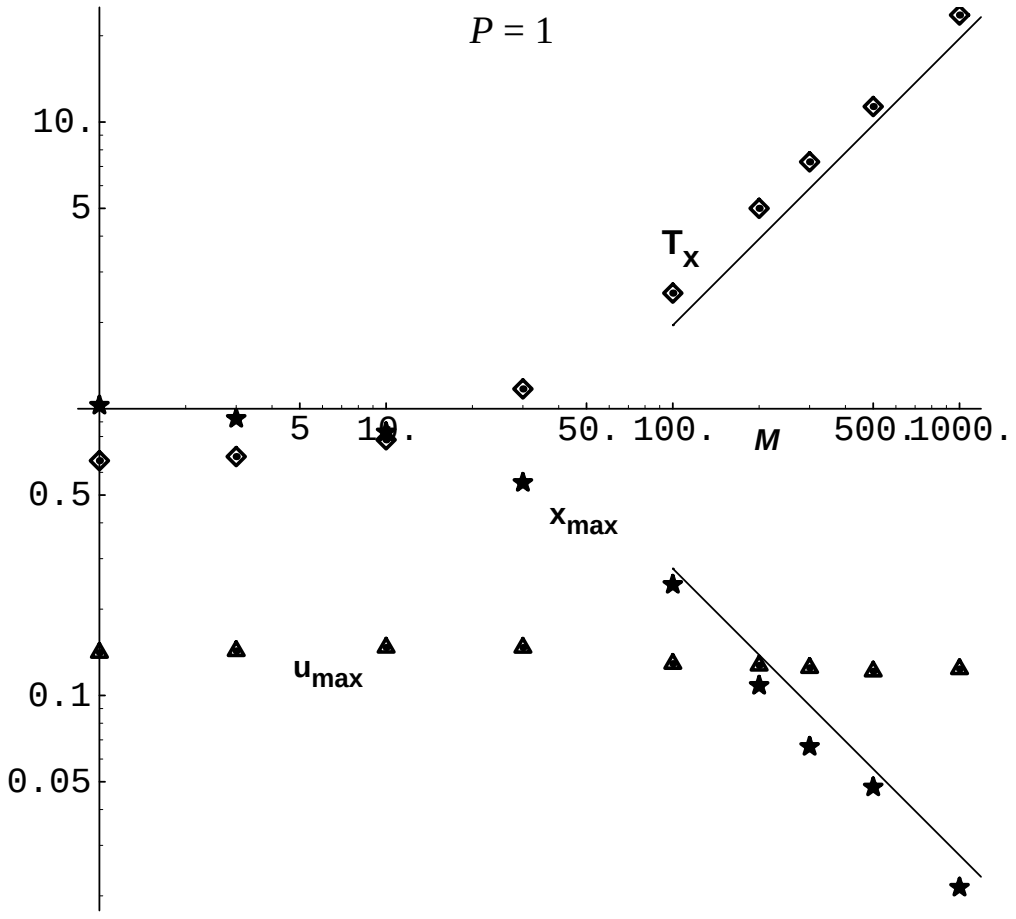

Figure 8: (b) $P = 1$.

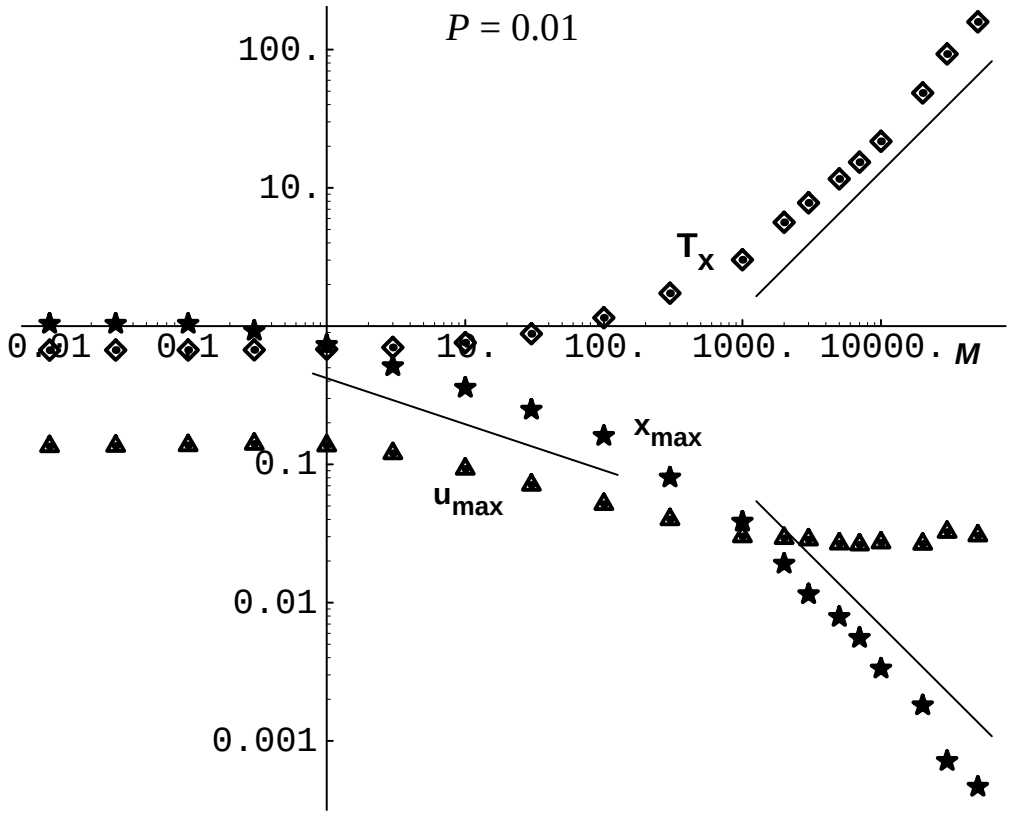

Figure 8: (c) $P = 0.01$.

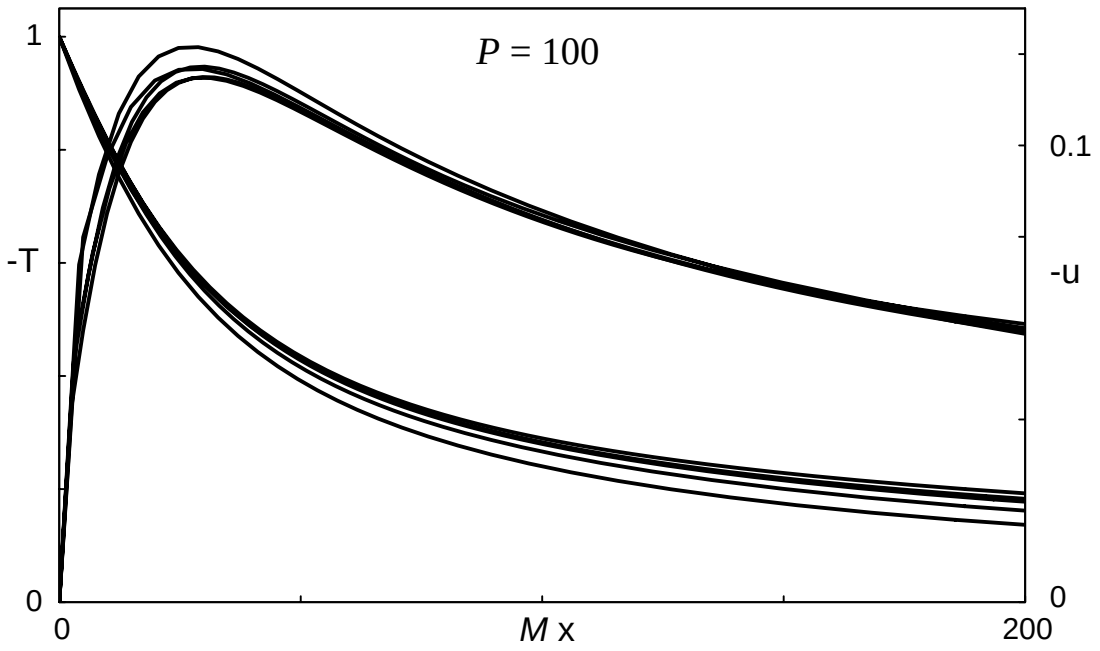

Figure 9: Rescaled Surface Profiles: temperature and velocity profiles for convective regimes, with x axis rescaled by M. The collapse of the data indicates the behavior in the cold corner is locally determined. (a) viscous case: $P = 100$; $M = 200$, 300, 500, 700, 1000.

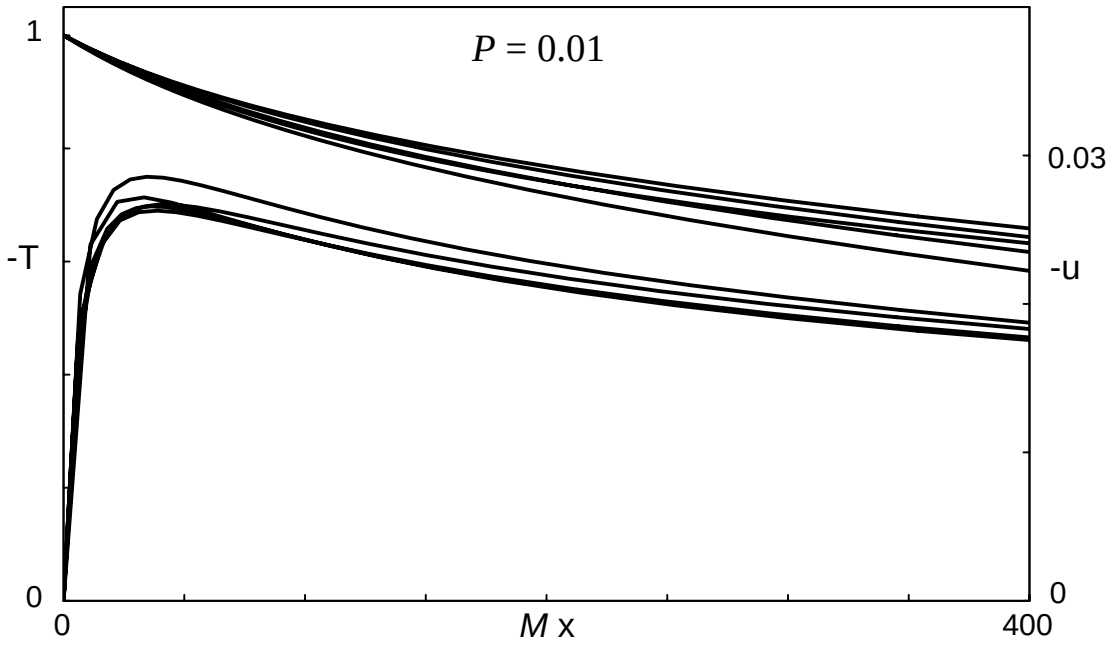

Figure 9: (b) inertial case: $P = 0.01$; $M = 3000$, 5000, 7000, 10,000, 20,000.